This is an open access article published under an ACS AuthorChoice License, which permits copying and redistribution of the article or any adaptations for non-commercial purposes.

ACS OMEGA

Article

Cite This: ACS Omega 2019, 4, 18370−18380

http://pubs.acs.org/journal/acsodf

Study of the Relationship Between Chlorhexidine-Grafted Amount and Biological Performances of Micro/Nanoporous Titanium Surfaces

Shuang Wang,[†] Yuanmeng Yang,[†] Wei Li, Zichen Wu, Jiaojiao Li, Kehui Xu, Weibo Zhang, Xianyu Zheng, and Jialong Chen*

Stomatologic Hospital and College, Key Laboratory of Oral Diseases Research of Anhui Province, Anhui Medical University, Hefei, Anhui 230032, China

ABSTRACT: Biomaterial-associated infection and lack of sufficient osseointegration contribute to a large proportion of implant failures. Therefore, antibacterial and osseointegration-accelerating properties are important in implant surface design. In this study, a micro/nanoporous titanium surface was prepared through alkaline and heat treatments, covalently conjugated with aminosilane. Then, varying amounts of chlorhexidine (CHX) were covalently grafted onto the aminosilane-modified surface via glutaraldehyde to obtain different CHX-grafted surfaces. These as-prepared surfaces were evaluated in terms of their surface chemical composition, surface topography, CHX grafting amount, antibacterial activity, and osteoblast compatibility. The results showed that the CHX grafting amount increased with increasing CHX concentrations, leading to better antibacterial activity. CHX (1 mg/mL) resulted in the best antibacterial surface, which still retained good osteoblast compatibility. Meanwhile, competitive bacterial-cell adhesion analysis demonstrated that this surface has great value for osteoblast adhesion at the implant−bone interface even in the presence of bacteria. This effortless, easily performed, and eco-friendly technique holds huge promise for clinical applications.

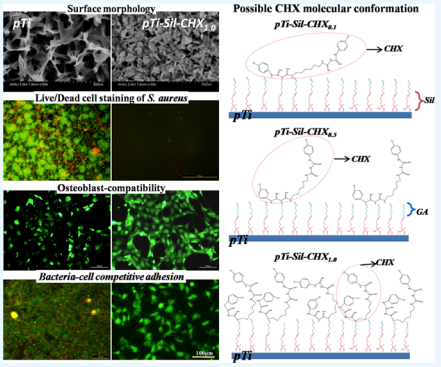

INTRODUCTION

Because of their excellent integrated performance (biocompatibility, mechanical properties, and low density), titanium and its alloys are considered to be the best materials for dental implants (DI).[1] However, during the early stages of implantation, peri-implant infections and poor osseointegration lead to the loss of tissue support for the implant and sometimes even treatment failure,[2] requiring costly rectification and often distressing the patient.

Planktonic bacteria first adhere onto the DI surface and then proliferate and produce extracellular polymeric substances, ultimately progressing to highly structured biofilms and leading to peri-implant infections involving peri-implant mucositis and peri-implantitis.[3,4] Upon biofilm formation on the biomaterial, the metabolism and antibiotic susceptibility of bacteria within the biofilm change such that the minimal inhibitory concentration of bacteria in the biofilm can increase by as much as 1000-fold for planktonic bacteria.[5] Through this defensive environment, bacteria have the capacity to evade the host's guards/safeguards and counter antibiotic attacks. Furthermore, biofilm-related antibiotic resistance might be intensified by the enhanced competence suggested for biofilm-embedded bacteria.[6] Then, a series of undesirable consequences can be triggered, including underlying life-threatening general infections, tissue damage, device failure/malfunction, and ultimately, removal of the implant. Compared with conventional approaches, including antibiotic therapy and surgical intervention, a better method to inhibit bacterial colonization and biofilm formation is to engineer implant surfaces with antibacterial coatings that prevent bacterial adherence and/or kill bacteria[7] These as-prepared coatings could allow drugs' loading in vivo at the implantation site, which antibiotics might have difficulty reaching,[8] increase retention time and lower drug dose levels to reduce unwanted side effects,[9] and maintain the bulk properties of the material.

Antibacterial coatings on DI surfaces are divided into drug-eluting coatings for the release of antibacterial agents to prevent bacterial adhesion and kill bacteria and permanent antibacterial coatings containing permanently bonded antibacterial drugs to prevent long-term bacterial adhesion. Antibacterial agents for delivery via drug-eluting coatings include (1) antibiotics such as gentamicin and vancomycin, (2) antiseptics such as chlorhexidine (CHX), and (3) metals such as silver and copper.[10,11] However, supratherapeutic levels of antibacterial drugs released from many elution coatings can be maintained for only a limited period of time, after which point, lower levels continue to be released for some time afterward.[12] This is problematic because an initial burst of drugs can be toxic to the already compromised bone[13] and transform a small fraction of bacteria into persistent cells, and the subsequent

Received: August 13, 2019
Accepted: October 10, 2019
Published: October 21, 2019

© 2019 American Chemical Society

DOI: 10.1021/acsomega.9b02614
ACS Omega 2019, 4, 18370−18380

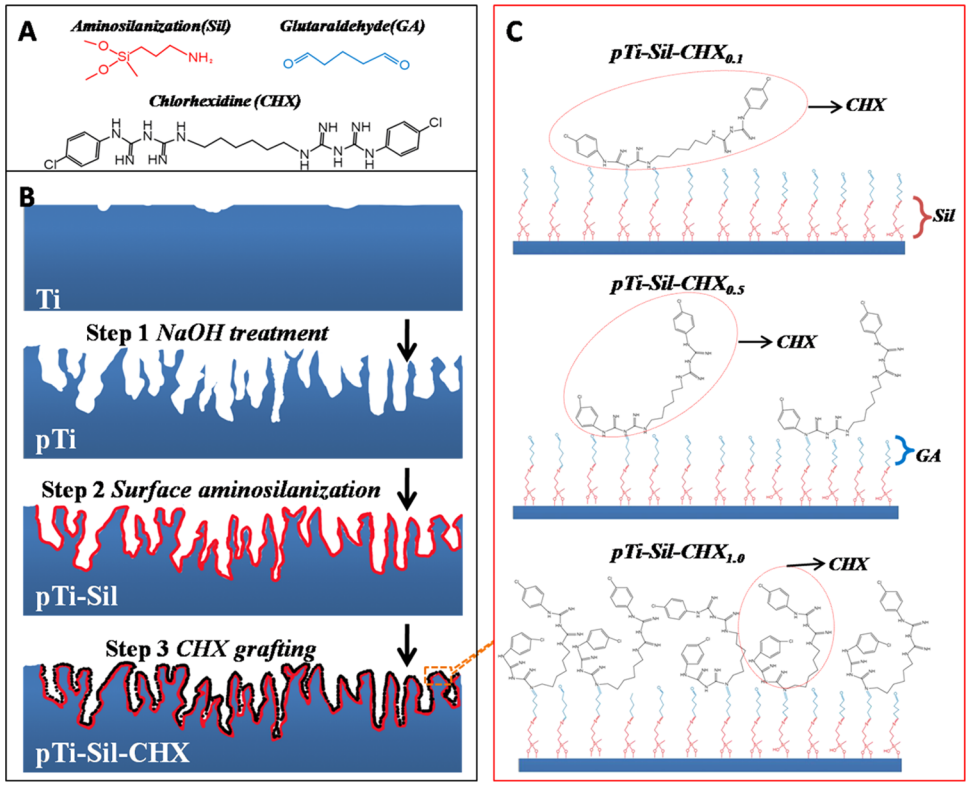

Figure 1. (A) Molecular structures of 3-aminopropyl(diethoxy)methylsilane (Sil), glutaraldehyde (GA), and chlorhexidine (CHX). (B) Illustration of the sample preparation processes. (C) Schematic of the possible molecular conformations of the grafted CHX on modified titanium in solutions with different CHX concentrations.

exponential decline in drugs to subtherapeutic levels can allow the bacteria to resume proliferation,[14] leading to antibiotic-resistant bacteria.[7] Permanent antibacterial coatings depend on covalently linked antibacterial drugs on the DI surface to destroy adherent bacteria. Compared with elution coatings, the amount of antibacterial agents on a permanent surface is small to reduce toxicity to the compromised bone.[15] However, the surface-bound drugs appear to retain their activity and exhibit good stability compared to free drugs,[16] and thus permanent surfaces can produce a long-term antibacterial environment. Tethered antibacterial compounds include various chitosans and quaternary ammonium salts,[7] antibacterial peptides,[17] and antibiotics.[18] Antibacterial compounds can be linked onto these surfaces by different cross-linkers including sulfhydryl bonds[19] and aminopropyltriethoxysilane.[20] However, when engineering an antibacterial coating, a balance must be maintained between the antibacterial property and cytocompatibility for implant−bone interfaces.

A three-dimensional micro/nanoporous structure possesses the typical features of native bone tissue, superior bioactivity, and inferior elastic modulus[1,21] to optimize the osteointegration of the DI through enlargement of the specific surface area to improve osteoblast proliferation and differentiation and bone ingrowth.[22,23] Even though the surface structure is an important factor in osteointegration, the implant is rendered extremely susceptible to bacterial colonization and subsequent biofilm formation due to the large surface area created by the overall open porosity and pore size.[2] Therefore, it is important to prepare DI surfaces that couple both a porous structure to promote osseointegration and antibacterial properties to prevent infection.

With its wide-spectrum antibacterial activity in physiological environments, chlorhexidine (CHX) has been utilized in clinical treatments as a topical antimicrobial, scrub agent, and lavage fluid,[24] and has been described as a good candidate for the development of materials and devices with antibacterial properties that do not encourage microbial evolution similar to antibiotic resistance, which is of acute concern to the global community.[25] CHX has been loaded into hydroxyapatite nanocapsules[26] or incorporated into polymeric systems[27] to sustain its release. However, only a few studies have utilized covalent linkage to graft CHX onto materials to prevent biomaterial-associated infection. Daud et al. reported that tethering CHX onto 316LSS via polydopamine had a long-term antibacterial effect, but there was no mention of cytocompatibility.[28] Aminosilanes are used extensively to bond biomolecules onto different materials via hydroxyl groups on the surface,[29] and our previous study involved covalent bonding of aminopropyltriethoxysilane to metal oxides to form a self-assembled monolayer with numerous amine groups. These amines can act as a starting point for covalent grafting with poly(ethylene glycol) to endow the surface with antifouling properties.[30,31]

Therefore, the present study aimed to build porous titanium surfaces modified with aminosilanes and covalently grafted with different amounts of CHX and then evaluate the antibacterial activity and osteoblast-compatibility performance of surface with given amounts of CHX. For this purpose, an aminosilane was applied for modification of a porous titanium substrate obtained by alkaline treatment. Then, varying amounts of CHX were covalently grafted onto the aminosilane-modified surface via glutaraldehyde (Figure 1B). Finally, the antibacterial properties and osteoblast compatibility of the

DOI: 10.1021/acsomega.9b02614
ACS Omega 2019, 4, 18370−18380

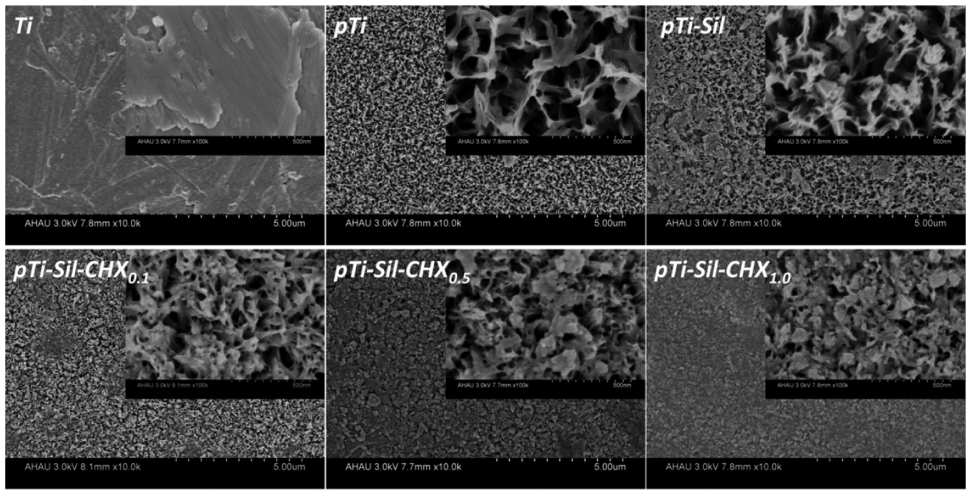

Figure 2. Surface morphologies of Ti, pTi, pTi-Sil, pTi-Sil-$CHX_{0.1}$, pTi-Sil-$CHX_{0.5}$, and pTi-Sil-$CHX_{1.0}$.

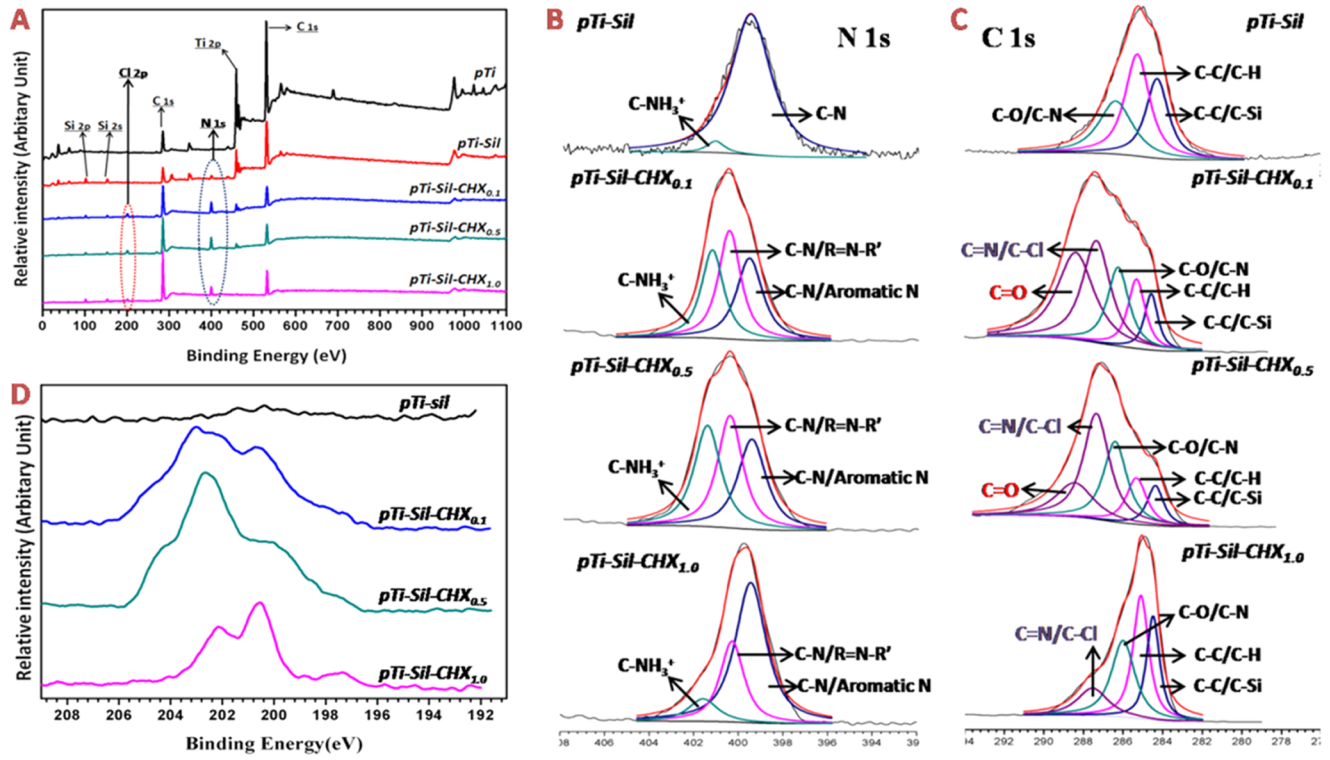

Figure 3. XPS wide scans (A) and high-resolution spectra of N 1s (B), C 1s (C), and Cl 2p (D) for the different surfaces.

resulting titanium surfaces were evaluated in vitro to forecast the retention of the coating after implantation. This method, through which implant surfaces with efficient antibacterial activity and bioactivity can be constructed, will have an impact on dental and relevant orthopedic fields.

RESULTS AND DISCUSSION

Surface Characterization. The surface morphologies of Ti, pTi, pTi-Sil, pTi-Sil-$CHX_{0.1}$, pTi-Sil-$CHX_{0.5}$, and pTi-Sil-$CHX_{1.0}$ are shown in Figure 2. Compared with compact flat titanium (Ti), NaOH treatment created a uniform micro/nano porosity and a mesh-like surface topography (pTi), leading to a large surface area. Kozlovsky et al. suggested that an increase in surface roughness was beneficial for CHX absorption and then demonstrated the substantial antibacterial effect provided through enlargement of the surface area.[32] Silanization (pTi-Sil) reduced the pore size, and then the grafted CHX (pTi-Sil-CHX) further reduced the pore size with increasing CHX concentrations. Daud et al. also reported that the amount of CHX adsorption on substrates increases with the CHX concentration, and the adsorbed CHX from higher CHX concentration solutions forms more/larger CHX aggregates to cover the surface.[28]

X-ray photoelectron spectroscopy (XPS) was used to analyze the chemical compositions of surfaces in different phases. The XPS wide-scan spectra of pTi, pTi-Sil, pTi-Sil-$CHX_{0.1}$, pTi-Sil-$CHX_{0.5}$, and pTi-Sil-$CHX_{1.0}$ are shown in Figure 3A. The XPS wide-scan spectrum of pTi-Sil showed the presence of N 1s, Si 2s, and Si 2p peaks and a decrease in the Ti 2p peak, indicating that aminosilane was successfully coated

DOI: 10.1021/acsomega.9b02614
ACS Omega 2019, 4, 18370−18380

onto the titanium surface. CHX conjugation to the aminosilanized surface led to a reduction in the Ti 2p and Si peaks, an increase in the N 1s peaks, and the presence of Cl 2p peaks, demonstrating that CHX was successfully grafted onto the surface of pTi-Sil. To illustrate the reaction mechanisms of CHX conjugation, N 1s (Figure 3B) and C 1s (Figure 3C) peak fittings were further carried out, and the detailed information is shown in Table 1. Compared with the spectrum of pTi-Sil, a new peak in the high-resolution N 1s spectra at ~400.5 eV (Figure 3B and Table 1/N2) and a new peak in the high-resolution C 1s spectra at ~287.4 eV (Figure 3C and Table 1/C4) occurred for pTi-Sil-CHX, which was consistent with the formation of C−N/R═N−R′ groups and C═N/C−Cl groups, illustrating that CHX was successfully grafted onto the surface. Among the three CHX-grafted surfaces, the area percentage of C−N/aromatic N (399.6 eV, Table 1/N1) in N 1s and C−C (284.6 and 285.6 eV, Table 1/C1 and C2) in C 1s with 62.9 and 56.1%, respectively, were both the highest for pTi-Sil-$CHX_{1.0}$, while that of C═N/C−Cl (287.7 eV, Table 1/C4) in total C 1s was the lowest, with only 14%, indicating that the benzene rings were exposed on the top surfaces rather than the guanidyl groups (Figure 1B). After immobilization of CHX, a new peak of C═O (288.4 eV, Table 1/C5) appeared in pTi-Sil-$CHX_{0.1}$ and pTi-Sil-$CHX_{0.5}$ (Figure 3C), which corresponded to the C═O groups in glutaraldehyde, but the proportion of this peak decreased from 32.7 to 17% when the concentration of CHX rose from 0.1 to 0.5 mg/mL, and the peak disappeared in pTi-Sil-$CHX_{1.0}$. Chances are that with a higher CHX dose, more reactions occurred between the C═O groups in glutaraldehyde and the guanidyl in CHX, thus leading to an increased grafting amount of CHX on the surfaces. The high-resolution Cl 2p spectra of the pTi-Sil-CHX surface at 202.4 eV for Cl $2p_{1/2}$ and 200.8 eV for Cl $2p_{3/2}$ further illustrated that CHX was successfully grafted onto the surface (Figure 3D). The Cl 2p spectra of pTi-Sil-$CHX_{1.0}$ were found to be different from that of pTi-Sil-$CHX_{0.1}$ and pTi-Sil-$CHX_{0.5}$, while the Cl 2p spectrum of pTi-Sil-$CHX_{1.0}$ was in agreement with a previous report investigating CHX-modified 316 L stainless-steel surfaces prepared by soaking dopamine-coated stainless steel in 44.9 mg/mL of CHX solution,[33] indicating that the molecular conformation of the grafted CHX changed with the CHX concentration.

The chemical elemental semiquantitative results of the different surfaces from the high-resolution spectra are shown in Table 2. Compared with pTi and pTi-Sil, a sharp decline in the titanium content and steep increases in the carbon and nitrogen contents were observed on the aminosilanized surface, demonstrating that the aminosilane was coated on the top of the Ti surface. Successful CHX incorporation onto the aminosilanized surface was demonstrated by decreases in the oxygen and titanium content, as well as significant increases in the carbon, nitrogen, and chlorine contents. Because there is no oxygen in CHX, the oxygen content decreased as the CHX solution concentration increased in the CHX-decorated surface groups, indirectly indicating that the CHX grafting amount increased as the concentration of the CHX solution increased. Meanwhile, the nitrogen content decreased and the carbon content increased with increasing CHX concentrations, also indicating that the molecular conformation of CHX changed to expose the benzene rings on the top surface and embed guanidyl into the subsurface. The N/Cl ratios of pTi-Sil-$CHX_{0.1}$, pTi-Sil-$CHX_{0.5}$, and pTi-Sil-$CHX_{1.0}$ were calculated to be 4.95, 5.40, and 7.07, respectively. A previous study reported that the N/Cl ratio of a CHX-decorated surface prepared at a CHX concentration of 44.9 mg/mL was calculated to be 7, which is in good agreement with the results of the sample of pTi-Sil-$CHX_{1.0}$.[33] Because the theoretical stoichiometric ratio of CHX is 5, the high N/Cl ratio of pTi-Sil-$CHX_{1.0}$ indicated that the molecular conformation of the grafted CHX on pTi-Sil-$CHX_{1.0}$ was different from that on pTi-Sil-$CHX_{0.1}$ and pTi-Sil-$CHX_{0.5}$. Speculation regarding the molecular conformation of the grafted CHX on pTi-Sil-$CHX_{1.0}$ is that contortion leads to the exposure of the benzene ring on the top surface, covering the guanidyl group (Figure 1C).

The water contact angle (WCA) reflects the wettability of a substrate and has been used in a wide range of studies to assess the efficacy of surface modification methods. Figure 4A shows the WCA values of the different surfaces. Compared with the original Ti (82.5 ± 4.9°), the WCA value of pTi decreased sharply to 7.4 ± 0.3°. After silanization (pTi-Sil), the WCA value increased significantly to 121.9 ± 1.3°, but CHX made the surface hydrophilic, and the WCA value of pTi-Sil-CHX significantly decreased. With increasing CHX concentrations, there was an increase in the surface hydrophilicity, and the WCA values of pTi-Sil-$CHX_{0.1}$, pTi-Sil-$CHX_{0.5}$, and pTi-Sil-$CHX_{1.0}$ were 106.6 ± 3.3, 64.2 ± 5.9, and 39.5 ± 3.7°, respectively. These results indirectly indicate that aminosilane and CHX were successfully grafted onto the micro/nanoporous titanium surfaces.

The quantitative NH amounts on the surface obtained by labeling with AO II using a linear standard curve (optical density vs concentration) are shown in Figure 4B. Spectrometric analysis of the stained samples showed that the surface of pTi-Sil possessed the largest NH amount, indicating that aminosilane was successfully incorporated onto the micro/

Table 1. Binding Energies (eV) and Area Percentages (%) of the Deconvoluted XPS N 1s and C 1s Peaks in pTi-Sil, pTi-Sil-$CHX_{0.1}$, pTi-Sil-$CHX_{0.5}$, and pTi-Sil-$CHX_{1.0}$

peak	binding energy (eV)	peak assignment	area percentage of peak (%) pTi-Sil	pTi-Sil-$CHX_{0.1}$	pTi-Sil-$CHX_{0.5}$	pTi-Sil-$CHX_{1.0}$
N1	~399.6	C−N, aromatic N	97.7	33	31.6	62.9
N2	~400.5	C−N, R═N−R′	0	36.9	35	27.6
N3	~401.7	C−NH_3^+	2.3	30.1	33.4	9.5
C1	~284.6	C−C, C−Si	29.5	8.2	8.9	23.4
C2	~285.6	C−C, C−H	40.9	12.4	12.6	32.7
C3	~286.2	C−O, C−N	29.6	17.5	25	29.9
C4	~287.4	C═N, C−Cl	0	29.2	36.5	14
C5	~288.4	C═O	0	32.7	17	0

Table 2. Elemental Composition and Ratios of Different Surfaces as Determined by XPS

samples	elements (atom %) C	O	N	Cl	Ti
pTi	27.59	50.11	2.26	0	20.04
pTi-Sil	35.72	47.47	4.58	0.27	11.96
pTi-Sil-$CHX_{0.1}$	63.6	17.89	12.88	2.6	3.03
pTi-Sil-$CHX_{0.5}$	67.73	15.37	12.7	2.35	1.85
pTi-Sil-$CHX_{1.0}$	75.94	14.6	8.13	1.15	0.18

DOI: 10.1021/acsomega.9b02614
ACS Omega 2019, 4, 18370−18380

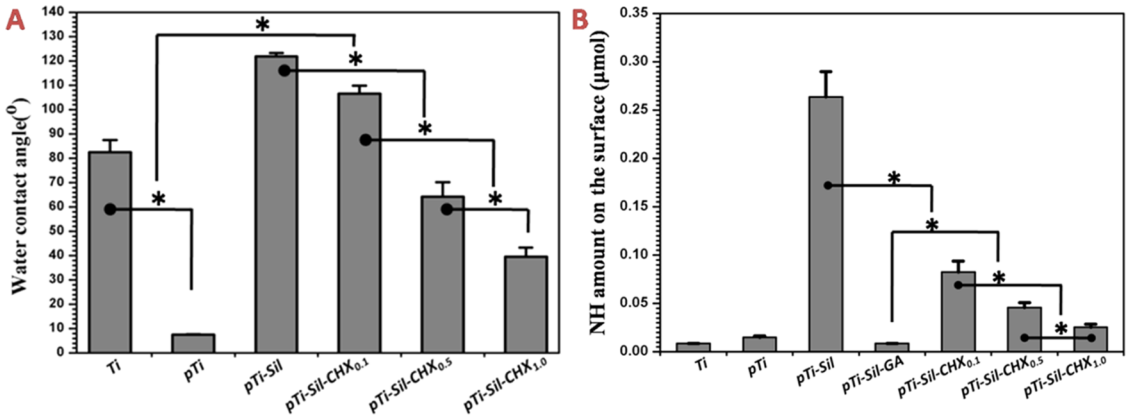

Figure 4. (A) Water contact angles of different surfaces. (B) Quantification of NH groups measured by the AO II method

nanoporous titanium surfaces. However, the NH groups on pTi-Sil were entirely consumed after glutaraldehyde treatment (pTi-Sil-GA), and a schematic of the possible GA linkage on the titanium surface is shown in Figure 1C. Thus, the NH content on the CHX-grafted surfaces was derived from the CHX molecules. Compared with pTi-Sil-GA, the NH amount on CHX-grafted surfaces significantly increased, but significantly decreased as the concentration of the CHX solution increased, indicating that CHX was successfully grafted onto micro/nanoporous titanium surfaces and that molecular contortion occurred much more frequently in the high CHX concentration group than in the low-concentration group, leading to exposure of the benzene ring on the top surface, which obscured the guanidyl group.

Quantification of the CHX grafted on the surfaces determined via UV−vis with a linear standard curve (optical density vs concentration) is shown in Table 3. The CHX grafting amount increased as the concentration of the CHX solution increased and was 0.44 ± 0.15 μg for pTi-Sil-$CHX_{0.1}$, 2.59 ± 0.42 μg for pTi-Sil-$CHX_{0.5}$, and 3.98 ± 0.31 μg for pTi-Sil-$CHX_{1.0}$ because higher CHX concentrations facilitated the formation of more/larger CHX aggregates and then led to higher CHX immobilization.[28] Meanwhile, the utilization rates of CHX in the solution for surface grafting were 2.2% for pTi-Sil-$CHX_{0.1}$, 2.59% for pTi-Sil-$CHX_{0.5}$, and 2% for pTi-Sil-$CHX_{1.0}$, which were far higher than the approximately 1% reported in a previous study.[28] Thus, the CHX application amount and utilization rate in this method led to less waste compared with the method used in the previous study.

Table 3. CHX Grafting Amount on the Surfaces and Utilization Rate of the CHX Solution

sample	CHX grafting amount (μg)	utilization rate of CHX solution (%)
pTi-Sil-$CHX_{0.1}$	0.44 ± 0.15	2.2
pTi-Sil-$CHX_{0.5}$	2.59 ± 0.42	2.59
pTi-Sil-$CHX_{1.0}$	3.98 ± 0.31	2.00

Antibacterial Activity. Adherence of bacteria to implanted devices and planktobacteria around implanted devices can lead to biomaterial-associated infections, often resulting in severe disease and implant failures. The antibacterial activity of the different samples in the local environment was investigated via zone of inhibition (ZOI) and optical density measurements. Clear transparent circles (inhibition zone) were observed around the CHX-grafted surfaces, and the size of the circles increased as the concentration of the CHX solution increased, showing the antibacterial effects of these surfaces (Figure 5A). Monitoring of the bacterial growth in solution was carried out by measuring the optical density at 660 nm (OD660) (Figure 5B). The higher the OD, the greater the opacity, based on the turbidity of the cell suspension. Compared with the surfaces without CHX, the CHX-grafted surfaces exhibited strong inhibition of *Staphylococcus aureus* growth after 24 h of culture, but the antibacterial activity of pTi-Sil-$CHX_{0.1}$ disappeared after 48 h of culture. On the other hand, when the CHX concentration was raised to 0.5 and 1.0 mg/mL, the sample surfaces still inhibited bacterial growth after 48 h. However, the antibacterial effect of pTi-Sil-$CHX_{1.0}$ was found to not only last longer but to be stronger because it almost entirely restrained bacteria growth.

Bacterial adherence to implanted materials can lead to biomaterial-associated infections, often causing severe complications and implant failures. The antibacterial activity of the different surfaces was investigated using live/dead bacteria staining and the plate counting method. Here, an in situ viability assessment of bacteria was carried out using a commercially available kit for live/dead bacterial fluorescence staining after 24 h of cultivation on various surfaces. As shown in Figure 6, the samples of Ti, pTi, and pTi-Sil supported rapid and extensive attachment of *S. aureus*. However, the number of bacteria adhered on the pTi-Sil was less than that on the pTi, and the percentages of apoptotic cells (yellow) and dead cells (red) were higher than those on the pTi, indicating that the positive charge increased the antibacterial activity.[34] Meanwhile, attachment onto the CHX-grafted surfaces was reduced by more than 80% compared with that on the pTi. Most of the bacterial cells on the CHX-grafted surfaces were dead (stained red), which was indicative of the high efficiency of CHX modification in prevention of bacterial adhesion and in killing of adherent bacteria. Among the CHX-grafted surfaces, the number of adhered bacteria decreased as the concentration of the CHX solution increased. CHX (1 mg/mL) produced the best antibacterial surface with the lowest number of bacteria and the highest proportion of dead bacterial. The number of bacteria on the different surfaces was determined by the dilution and plate counting method. After 24 h of culture, the bacteria adhered on the samples were dispersed into phosphate-buffered saline (PBS) and then cultured on the

DOI: 10.1021/acsomega.9b02614
ACS Omega 2019, 4, 18370−18380

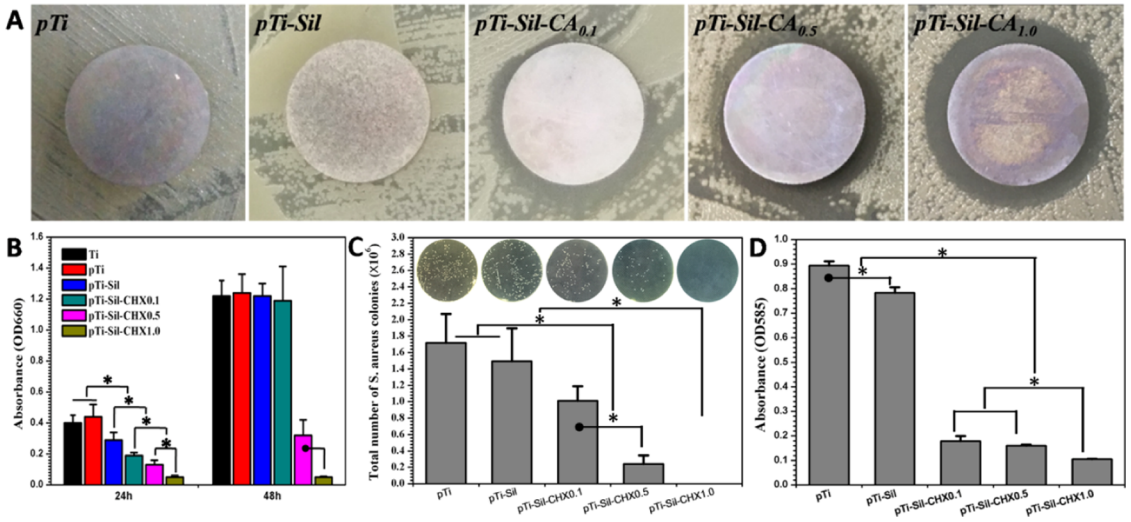

Figure 5. (A) Zone of inhibition (ZOI) testing of the different samples against *S. aureus*. (B) Bacterial growth curves of *S. aureus* in LB medium incubated with the different samples. (C) Plate count of *S. aureus* adhered onto the different samples (subset: photograph of bacteria colonies on the solid LB agar plates). (D) Biofilm formation by *S. aureus* on different surfaces, measured using the crystal violet method.

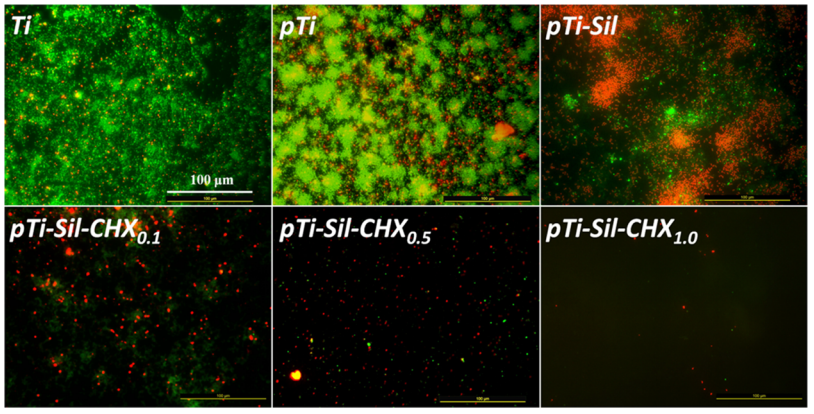

Figure 6. Fluorescence images of *S. aureus* on the different surfaces, visualizing live cells (green), dead cells (red), and apoptotic cells (yellow).

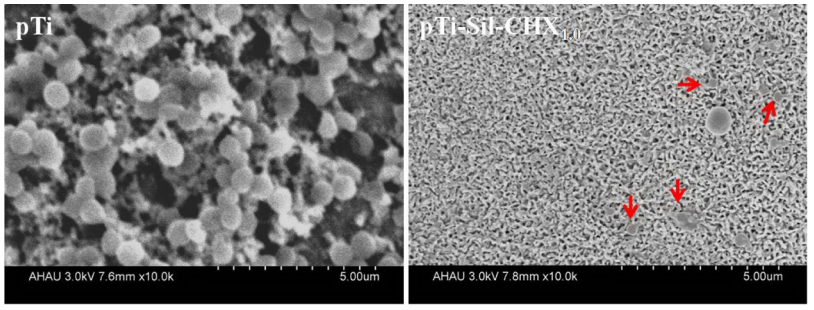

Figure 7. SEM photographs of *S. aureus* on pTi and pTi-Sil-CHX$_{1.0}$ after 48 h of incubation.

surface of solid LB agar plates for visible testing of the bacteria count (Figure 5C). Bacterial colonies were visibly observed in connection with pTi and pTi-sil, but the number of bacterial colonies decreased with increasing concentrations of CHX in the CHX-decorated surface groups. The colony-forming unit (CFU) number of pTi-Sil-CHX$_{0.1}$ ($(1.01 \pm 0.18) \times 10^6$) decreased slightly compared to pTi ($(1.72 \pm 0.35) \times 10^6$) and pTi-Sil ($(1.49 \pm 0.40) \times 10^6$), while pTi-Sil-CHX$_{0.5}$ ($(0.24 \pm 0.11) \times 10^6$) caused significant reduction. The highest reduction was noted for pTi-Sil-CHX$_{1.0}$, without any CFU counted. This result also demonstrated that 1 mg/mL of CHX produced the best antibacterial surface with the lowest number of live bacteria.

The results of assessments of the adherence of bacteria onto the titanium surface and the bacteria growth in the local environment indicated that the grafted CHX improved the antibacterial activity of the samples and that the inhibitory effect was enhanced with an increase in the CHX grafting amount. The greatest antibacterial effect was observed when the surface was prepared with a CHX solution concentration of 1 mg/mL. Previous studies have also suggested that CHX-decorated surfaces possess excellent antibacterial proper-

DOI: 10.1021/acsomega.9b02614
ACS Omega 2019, 4, 18370−18380

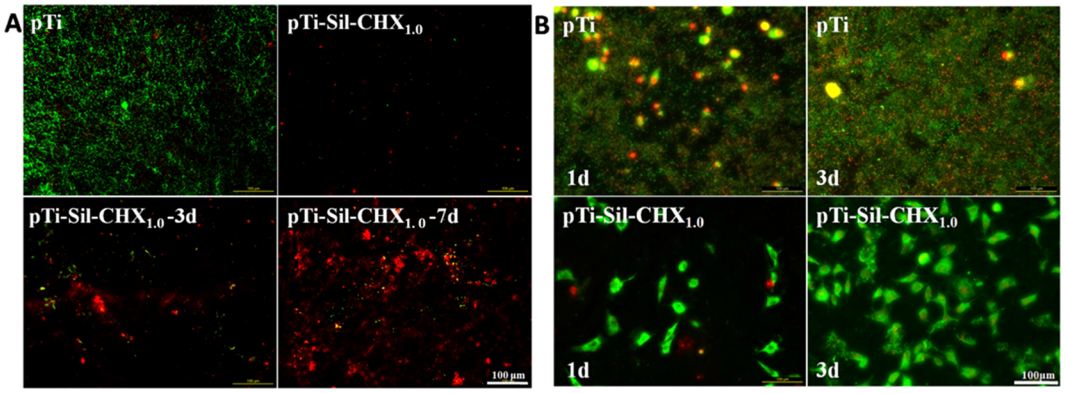

Figure 8. (A) Fluorescence images of *S. aureus* on pTi and pTi-Sil-$CHX_{1.0}$ surfaces before and after immersion in PBS for 3 and 7 days, visualizing live cells (green), dead cells (red), and apoptotic cells (yellow). (B) Fluorescence images of *S. aureus* and osteoblast cocultivation on pTi and pTi-Sil-$CHX_{1.0}$ surfaces after 1 and 3 days of culture.

ties,[28,33,35] but the CHX concentration in these studies was far higher than 1 mg/mL. Therefore, our study provides evidence that the use of such high CHX concentration solutions to prepare the CHX-decorated surfaces is unnecessary; still, an excessively low concentration of CHX is inadequate to produce a satisfactory antibacterial surface.

Because bacterial biofilms are inherently resistant to antibiotics and the human immune system, bacterial biofilms may lead to treatment failure as a consequence of persistent infection. To evaluate the ability of the surfaces to inhibit biofilm formation, biofilms were formed using an *S. aureus* monospecies biofilm model and then were examined by the colorimetric measurement of crystal violet incorporation by sessile cells (Figure 5D). The biofilm amount formed on pTi and pTi-Sil surfaces was higher than that on the CHX surfaces, confirming the efficacy of CHX to impede the formation of bacterial biofilms on the material surfaces. Furthermore, the suppression of biofilm formation varied among the experimental groups according to the usage of CHX (0.1, 0.5, 1.0 mg/mL), and pTi-Sil-$CHX_{1.0}$ was found to have the best inhibitory effect.

Scanning electron microscopy (SEM) photographs of *S. aureus* on pTi and pTi-Sil-$CHX_{1.0}$ in vitro after 48 h of incubation are shown in Figure 7. A thick biofilm formed on the pTi surface, covering the micro/nanoporous titanium surface, whereas the surface of pTi-Sil-$CHX_{1.0}$ retained its porous structure. Moreover, pTi-Sil-$CHX_{1.0}$ exhibited an antibiofilm effect and disrupted biofilm formation, and most of the adherent *S. aureus* were dead (red arrows).

To evaluate the stability of the coating, the samples of pTi-Sil-$CHX_{1.0}$ were immersed in PBS for 3 and 7 days and then their antibacterial properties were assessed via live/dead bacteria staining (Figure 8A). The number of bacteria adhered on the CHX-modified surfaces was far less than that on the pTi surface, indicating that the CHX-modified surfaces with or without immersion in PBS possessed antibacterial activity. However, with increasing immersion times in PBS, the amount of bacteria on pTi-Sil-$CHX_{1.0}$-3d and pTi-Sil-$CHX_{1.0}$-7d greatly increased, indicating that the antibacterial activity of these surfaces decreased. We speculate that hydrolysis of the silanes might result in a decrease in the amount of CHX bound on the material surface.[36] However, the percentages of apoptotic cells (yellow) and dead cells (red) on pTi-Sil-$CHX_{1.0}$-3d and pTi-Sil-$CHX_{1.0}$-7d were higher than those on pTi, indicating that these surfaces still had good bactericidal activity. To some extent, the lasting sterilization might remedy the defect in inhibition of bacterial adhesion, and thus, the antibacterial activity did not appear to decrease with an extension of immersion time. However, although the number of adherent bacteria on the surface continued to grow, the early stage of healing can be achieved within 5 days; a previous study reported that an initial mucosal seal could be established by the 4th day after the implant placement.[37] In addition, silane hydrolysis might expose the porous substrate to promote bone integration.[22,23]

Osteoblast Compatibility. Many antibacterial agents that can endow dental implants with antibacterial activity have been actively studied too, but these agents lack biocompatibility.[30,38] Cytotoxicity and internal organ injury[2,39] caused by the as-prepared surfaces are problems that must be solved.[40,41] The cytotoxicity toward the mouse osteoblast-like MC3T3-E1 cell line, as another crucial factor, should be evaluated with caution once a newly modified Ti is used as a DI. Figure 9 shows the in

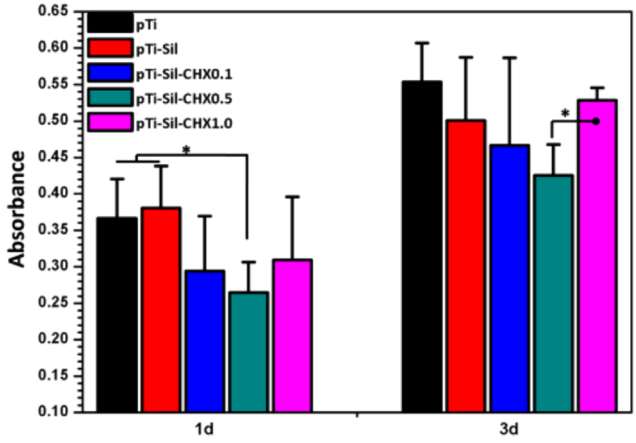

Figure 9. Osteoblast proliferation on different surfaces after culture for 1 and 3 days, as determined by an MTT assay

vitro cell viability cultured with the different samples in Dulbecco's modified Eagle's medium for 1 and 3 days, assessed with an 3-(4,5-dimethylthiazol-2-yl)-2,5-diphenyltetrazolium bromide (MTT) assay. The viability of cells cultured on pTi was higher than that of those cultured on the CHX-decorated Ti surfaces, indicating that modification of the Ti surface with CHX led to some cytotoxicity that affected cell adhesion and proliferation, but only the viability of cells grown pTi-Sil-

DOI: 10.1021/acsomega.9b02614
ACS Omega 2019, 4, 18370−18380

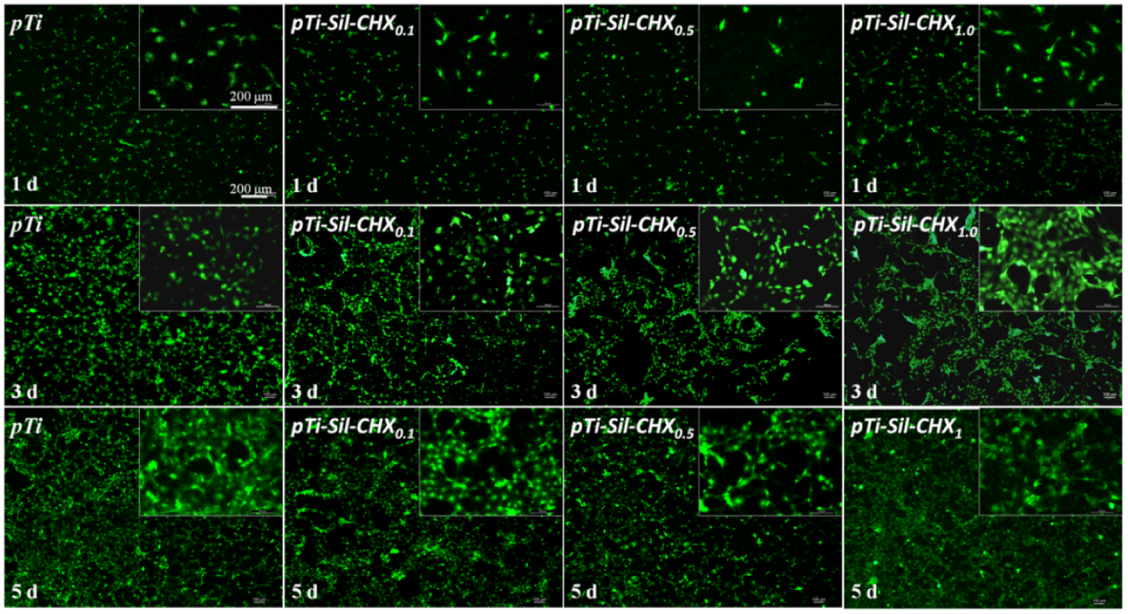

Figure 10. Rhodamine123 staining of osteoblasts (MC3T3-E1) cultured on different surfaces after 1, 3, and 5 days of culture

$CHX_{0.5}$ for 1 day showed significant differences from the pTi group. After 3 days of incubation, the pTi groups still showed higher cell viability than the CHX-grafted Ti counterparts, but the cells cultured with these samples showed no significant differences in cell viability. Among the three types of CHX-grafted Ti, cells on the pTi-Sil-$CHX_{1.0}$ maintained better viability at all times, and at 3 days, the viability value was very similar to that of cells on the pTi.

To observe the morphologies of the cells adhered on the different surfaces after 1, 3, and 5 days of culture, rhodamine123 was used to stain the cellular matrix (Figure 10). As the culture time increased, the number of cells attached on each sample grew. After 1 day of culture, the sizes and numbers of adherent cells on the pTi and pTi-Sil-$CHX_{1.0}$ were greater than those on other surfaces. Meanwhile, the number of adherent cells on pTi-Sil-$CHX_{0.5}$ was less than that on the other surfaces, which indicated that this surface was not favorable for osteoblast adhesion. After 3 days of culture, the number of cells adhered on each sample increased, and the adhered cells spread pseudopodia and had healthy spindle shapes, but adhered cells on the CHX-grafted Ti were unevenly distributed throughout the surface. Compared with pTi, a nearly equal amount of cells could be observed on pTi-Sil-$CHX_{1.0}$ and the cells covered nearly the entire surface at 5 days, indicating that the CHX-decorated surface at a concentration of 1.0 mg/mL did not inhibit cell attachment or growth on the Ti substrates. Meanwhile, the cells on pTi-Sil-$CHX_{0.1}$ and pTi-Sil-$CHX_{0.5}$ were flattened and exhibited a smaller attachment area than the other samples, which was in accordance with the MTT results. One possible reason for the good cytocompatibility of pTi-Sil-$CHX_{1.0}$ is that the benzene ring of the grafted CHX on pTi-Sil-$CHX_{1.0}$ is exposed on the top surface and covers the guanidyl group, resulting in surfaces with a low positive charge.

Competitive Bacterial-Cell Adhesion. During the implantation operations, bacteria can be brought into the implant−bone interface by the implant, saliva, and blood, which leads to infection. To simulate the possible problems caused by infection during the clinical implantation process, samples were incubated with bacteria and cells in sequence to evaluate the importance of surface modification. The results showed that the pTi surface was occupied by a large number of bacteria and a small number of cells (Figure 8B) after 1 day of coculture, and most of the cells exhibited red fluorescence, indicating that the cells had been destroyed. Conversely, the CHX-grafted surface was covered by a large number of green (living) cells with good cell morphology, and very few dead bacterial cells (stained red) were observed. The surface of pTi-Sil-$CHX_{1.0}$ exhibited high efficiency in destroying the bacterial cells and supported cell adhesion. After 3 days of coculture, a thick biofilm and very few apoptotic cells (stained yellow) were observed on the pTi surface, while a large number of cells but no bacteria were observed on the pTi-Sil-$CHX_{1.0}$, and the adhered cells exhibited spread pseudopodia and a healthy spindle shape. These results demonstrate that in the cell-bacteria competition environment, if the bacteria cannot be effectively inhibited, rapid proliferation and colonization occur on the material surface, thereby restricting cell adhesion and even causing cell death.

CONCLUSIONS

Micro/nanoporous titanium surfaces grafted with different amounts of CHX using aminosilane and glutaraldehyde as chemical cross-linkers were evaluated in terms of the surface chemical composition, surface topography, CHX grafting amount, antibacterial activity, and osteoblast compatibility. CHX-grafted coatings were successfully prepared on micro/nanoporous titanium surfaces, while the CHX grafting amount increased with increasing CHX concentrations, further leading to better antibacterial activity. CHX (1 mg/mL) yielded the best antibacterial surface, and this surface retained the good osteoblast compatibility of titanium. Bacterial-cell competitive adhesion assays demonstrated that the antibacterial surface of pTi-Sil-$CHX_{1.0}$ has great value for osteoblast adhesion at the implant−bone interface even in the presence of bacteria. Therefore, a CHX-grafted coating on the micro/nanoporous structure (pTi-Sil-$CHX_{1.0}$) may not only prevent infection but also retain good osteoblast compatibility for further osteointe-

DOI: 10.1021/acsomega.9b02614
ACS Omega 2019, 4, 18370−18380

gration of titanium implants. This effortless, easily performed, and eco-friendly technique holds huge promise for clinical applications.

EXPERIMENTAL SECTION

Materials. Commercial pure titanium (Ti) was purchased from Baoji Nonferrous Metal Co., Ltd. (Shanxi Province, China). 3-Aminopropyl(diethoxy)methylsilane (aminosilane), chlorhexidine acetate (CHX), glutaraldehyde, acid orange II (AO II), crystal violet, and rhodamine123 were purchased from Sigma-Aldrich. Fetal bovine serum and α-minimum Eagle's medium were purchased from Gibco. *S. aureus* and the mouse MC3T3-E1 cell line were purchased from ATCC.

Fabrication and Characterization of the CHX-Modified Surfaces. Titanium disks were polished to achieve a reflective, mirror-like surface, followed by ultrasonic cleaning first in acetone, then in ethanol and finally in deionized water. After immersion in a 5 M NaOH solution at 60 °C for 12 h, the cleaned specimens were immersed in boiling deionized water for 2 h (denoted pTi) and subsequently soaked in a 1% (v/v) ethanol solution of 3-aminopropyl(diethoxy)-methylsilane for 10 h at 37 °C with gentle shaking. After the reaction, the samples were ultrasonically cleaned with the same solvents and then kept in a 120 °C oven for 2 h to enhance binding of the aminosilane with the surface (denoted pTi-Sil). The samples of pTi-Sil were immersed in a 2% (v/v) glutaraldehyde solution for 4 h at room temperature (RT), and then, any ungrafted moieties on the surface were washed away with water (denoted pTi-Sil-GA). CHX at three different concentrations (0.1, 0.5, and 1 mg/mL) were grafted onto the surfaces separately by soaking the modified samples in 0.2 mL of CHX solution for 24 h. The CHX-grafted samples were washed with deionized water three times and then placed in a vacuum system for further use. The samples were denoted pTi-Sil-$CHX_{0.1}$, pTi-Sil-$CHX_{0.5}$, and pTi-Sil-$CHX_{1.0}$.

After coating with gold for 30 s, the surface topographies of the different samples were investigated using scanning electron microscopy (SEM, Hitachi S-4800). The surface chemical composition was analyzed via XPS (Thermo ESCALAB 250) at a pass energy of 100 eV over a wide scan with a binding energy (BE) range of 0−1400 eV; meanwhile, the elemental states of the different samples were analyzed at a pass energy of 30 eV to produce high-resolution detailed scans. The system was calibrated using the C 1s peak at 284.8 eV. Because the take-off angle was set to 45°, the investigation depth was no more than 10 nm. The Xpspeak software package was used to perform quantitative analysis and curve fitting for the collected data. The wettability of the different surfaces was investigated by measuring the water contact angle using deionized water at room temperature. Measurements were made on five samples from each group, and each sample was separately measured twice.

An improved AO II assay was performed to quantify the density of the surface amine groups (primary, secondary, and tertiary).[31] Two milliliters of AO II aqueous solution (500 μmol/L, pH 3) was incubated with the samples for 24 h at RT, and then the samples were removed from the solution and rinsed with water (pH 3) five times. Finally, the samples were shaken for 12 h in water (pH 12) to release the adsorbed AO II. A colorimetric method was applied to determine the AO II concentration of the solution using a microplate photometer (μQuant, BioTek, Winooski, VT) with an optical spectrometer at 485 nm. The amine amounts on the different surfaces were calculated according to a standard calibration curve (known AO II concentrations vs OD values).

The amounts of CHX grafted on the surfaces incubated with different CHX concentrations (0.1, 0.5, and 1 mg/mL) were evaluated by measuring the total reduction in CHX in the solution at a wavelength of 230 nm. After the reaction, the solutions in the centrifuge tubes containing the samples were shaken at 120 rpm for 1 h and then measured by a NanoDrop 2000 UV spectrophotometer (Thermo Scientific, Waltham, MA). The resulting data were calculated according to a standard calibration curve (known CHX concentration vs OD value).

Antibacterial Test. The capability of the CHX-grafted titanium to present antibacterial activity was assessed with *S. aureus*. *S. aureus* (ATCC 6538) was cultivated on a solid LB medium agar plate. After static incubation for 24 h at 37 °C, a colony was picked from the agar plate using a sterile inoculation loop and added into Luria−Bertani (LB) broth and then diluted to 10^7 CFU/mL to obtain a test strain solution.

First, the antibacterial activity of the samples was assessed using a zone of inhibition (ZOI) test.[2] 20 μL of each individual test strain solution was spread evenly onto a solid LB agar plate surface, and then the samples were lightly placed face down on the solid LB agar. After static incubation at 37 °C for 1 day, the apparent ZOI around the sample was photographed to assess the antibacterial activity of the modified surface. Then, 80 μL aliquots of the test inoculum were distributed onto the surfaces of different samples in a 24-well plate and gently covered with a piece of polyethylene film to spread the solution to the edges.[42] After incubation for 4 h at 37 °C, 1 mL of LB broth was added to each well and incubated with the samples in an orbital shaker incubator at 150 rpm and 37 °C for the following valuation. (1) After incubation for 24 and 48 h, 100 μL of LB broth was taken out and optical density was measured at 660 nm (OD_{660}) using a microplate reader. (2) After incubation for 24 h, the samples were taken out and gently rinsed with PBS. Then, both live and dead bacteria on the samples were stained using a LIVE/DEAD*Bac*Light Bacterial Viability Kit (Invitrogen, Carlsbad, CA) to assess the antibacterial properties of the different materials. Live bacterial cells were stained green, whereas dead cells were stained red. (3) After incubation for 24 h, each sample was taken out and gently rinsed with PBS and put into a sterilized centrifuge tube with 200 μL of PBS. After ultrasonic processing for 2 min and vortex processing for 5 min, 10 μL of the PBS in centrifuge tubes was collected and 10-fold serial dilutions were prepared using sterilized saline. Then, 100 μL aliquots were spread evenly onto a solid LB agar plate surface. After incubation for different times, the CFU on the plates were counted. (4) After incubation for 24 h, the samples were washed with PBS and fixed in 2.5% glutaraldehyde in PBS for 12 h. After they were dehydrated, dealcoholized, and dried, the fixed samples were observed via SEM. (5) After 72 h of incubation, the samples were taken out and washed twice with sterile PBS, and then stained with 400 μL of a 0.1% (v/v) crystal violet solution for 10 min. The excess crystal violet was rinsed with PBS. Then, 400 μL of a 7% acetic acid solution was added and shaken for 10 min. The absorbance of bacteria biofilms was measured in a 96-well plate at a wavelength of 595 nm.

Covalent immobilization stably links a molecule onto the surface for a long time. To evaluate the stability of the coating,

DOI: 10.1021/acsomega.9b02614
ACS Omega 2019, 4, 18370−18380

the CHX-modified samples in 2 mL of aseptic PBS solution were placed in an orbital shaker incubator at 150 rpm and 37 °C, and then taken out after 3 or 7 days. After being rinsed, dried, and sterilized with an ultraviolet lamp, the antibacterial properties of the samples were assessed via live and dead bacteria staining using the above-mentioned methods.

Cell Attachment and Proliferation. Mouse (MC3T3-E1) osteoblasts were cultured in a humidified incubator under 5% CO_2 at 37 °C using α-minimum Eagle's medium supplemented with 15% fetal bovine serum. When the cells reached 80−90% confluence, they were trypsinized, harvested by centrifugation, resuspended, and diluted to a density of 1×10^5 cells/mL. Then, 1 mL aliquots of the cell suspension were incubated with the as-sterilized samples in a 24-well plate at 37 °C and 5% CO_2. The samples were removed, moderately washed, and fixed with 2.5% glutaraldehyde after 1 and 3 days of incubation. Then, the samples were washed with PBS and incubated with rhodamine123 (20 μg/mL) for 15 min, after which they were immediately examined under a fluorescence microscope.[43] Cell proliferation was determined by an MTT assay after 1 and 3 days of cultivation.

Competitive Bacterial-Cell Adhesion. First, 80 μL of LB broth containing *S. aureus* (10^5 CFU) was distributed onto the different sterilized surfaces and incubated for 4 h at 37 °C. Then, the samples were rinsed with PBS once, and 1 mL aliquots of cell suspension (MC3T3-E1) with a density of 5×10^4 cells/mL were inoculated onto the samples. After incubation for 1 and 3 days at 37 °C, the samples were gently washed with PBS, and then both live and dead bacteria/cells on the samples were stained using the LIVE/DEAD*Bac*Light Bacterial Viability Kit to assess the competitive bacterial-cell adhesion to the different materials.

Statistics. Water contact angle, AO II, bacteria growth measurements, and the MTT assays were carried out independently at least three times using more than four parallel samples. The data are presented as the mean ± standard deviation and were compared through one-way analysis of variance using SPSS software to evaluate significant differences. In the figures, statistically significant differences ($p < 0.05$) are denoted with asterisks (*).

Ethical Statement. All experimental protocols were approved by the Ethical Committee of Anhui Medical University (protocol number: 20160126).

AUTHOR INFORMATION

Corresponding Author

*E-mail: jialong_dt@126.com. Tel: +8613721090114. Fax: +86-551-65161183.

ORCID

Jialong Chen: 0000-0002-5323-1801

Author Contributions

†S.W. and Y.Y. contributed equally to this work.

Notes

The authors declare no competing financial interest.

ACKNOWLEDGMENTS

This work was supported by the National Natural Science Foundation of China (no. 31670967), the Scientific Research Foundation of the Institute for Translational Medicine of Anhui Province (no. 2017zhyx19), the University Outstanding Youth Talent Support Program of Anhui Province (no. gxyq2018007), and the Postdoctoral Science Foundation of Anhui Province (no. 2018B264).

REFERENCES

(1) Chen, J. L.; Li, Q. L.; Chen, J. Y.; Chen, C.; Huang, N. Improving blood-compatibility of titanium by coating collagen-heparin multilayers. *Appl. Surf. Sci.* **2009**, *255*, 6894−6900.

(2) Chen, J.; Mei, M. L.; Li, Q. L.; Chu, C. H. Mussel-inspired silver-nanoparticle coating on porous titanium surfaces to promote mineralization. *RSC Adv.* **2016**, *6*, 104025−104035.

(3) Wang, R.; Neoh, K. G.; Shi, Z.; Kang, E. T.; Tambyah, P. A.; Chiong, E. Inhibition of escherichia coli and proteus mirabilis adhesion and biofilm formation on medical grade silicone surface. *Biotechnol. Bioeng.* **2012**, *109*, 336−345.

(4) Dastgheyb, S. S.; Hammoud, S.; Ketonis, C.; Liu, A. Y.; Fitzgerald, K.; Parvizi, J.; Purtill, J.; Ciccotti, M.; Shapiro, I. M.; Otto, M.; Hickok, N. J. Staphylococcal Persistence Due to Biofilm Formation in Synovial Fluid Containing Prophylactic Cefazolin. *Antimicrob. Agents Chemother.* **2015**, *59*, 2122−2128.

(5) Otto, M. Staphylococcal Infections: Mechanisms of Biofilm Maturation and Detachment as Critical Determinants of Pathogenicity. *Annu. Rev. Med.* **2013**, *64*, 175−188.

(6) Darouiche, R. O. Treatment of Infections Associated with Surgical Implants. *N. Engl. J. Med.* **2004**, *350*, 1422−1429.

(7) Hickok, N. J.; Shapiro, I. M.; Chen, A. F. The Impact of Incorporating Antimicrobials into Implant Surfaces. *J. Dent. Res.* **2018**, *97*, 14−22.

(8) He, T.; Shi, Z. L.; Fang, N.; Neoh, K. G.; Kang, E. T.; Chan, V. The effect of adhesive ligands on bacterial and fibroblast adhesions to surfaces. *Biomaterials* **2009**, *30*, 317−326.

(9) Borse, V.; Pawar, V.; Shetty, G.; Mullaji, A.; Srivastava, R. Nanobiotechnology Perspectives on Prevention and Treatment of Ortho-paedic Implant Associated Infection. *Curr. Drug Delivery* **2016**, *13*, 175−185.

(10) Jepsen, K.; Jepsen, S. Antibiotics/antimicrobials: systemic and local administration in the therapy of mild to moderately advanced periodontitis. *Periodontology 2000* **2016**, *71*, 82−112.

(11) Qi, L.; Liu, Z.; Wang, N.; Hu, Y. Facile and efficient in situ synthesis of silver nanoparticles on diverse filtration membrane surfaces for antimicrobial performance. *Appl. Surf. Sci.* **2018**, *456*, 95−103.

(12) Bormann, N.; Schwabe, P.; Smith, M. D.; Wildemann, B. Analysis of parameters influencing the release of antibiotics mixed with bone grafting material using a reliable mixing procedure. *Bone* **2014**, *59*, 162−172.

(13) Antoci, V. J.; Adams, C. S.; Hickok, N. J.; Shapiro, I. M.; Parvizi, J. Antibiotics for Local Delivery Systems Cause Skeletal Cell Toxicity In Vitro. *Clin. Orthop. Relat. Res.* **2007**, *462*, 200−206.

(14) Lewis, K. Persister Cells: Molecular Mechanisms Related to Antibiotic Tolerance. In *Antibiotic Resistance*; Coates, A. R. M., Ed.; Springer Berlin Heidelberg: Berlin, Heidelberg, 2012; pp 121−133.

(15) Antoci, V., Jr.; Adams, C. S.; Parvizi, J.; Ducheyne, P.; Shapiro, I. M.; Hickok, N. J. Covalently Attached Vancomycin Provides a Nanoscale Antibacterial Surface. *Clin. Orthop. Relat. Res.* **2007**, *461*, 81−87.

(16) Antoci, V., Jr.; Adams, C. S.; Parvizi, J.; Davidson, H. M.; Composto, R. J.; Freeman, T. A.; Wickstrom, E.; Ducheyne, P.; Jungkind, D.; Shapiro, I. M.; Hickok, N. J. The inhibition of Staphylococcus epidermidis biofilm formation by vancomycin-modified titanium alloy and implications for the treatment of periprosthetic infection. *Biomaterials* **2008**, *29*, 4684−4690.

(17) de la Fuente-Núñez, C.; Cardoso, M. H.; de Souza Cândido, E.; Franco, O. L.; Hancock, R. E. Synthetic antibiofilm peptides. *Biochim. Biophys. Acta, Biomembr.* **2016**, *1858*, 1061−1069.

(18) Hickok, N. J.; Shapiro, I. M. Immobilized antibiotics to prevent orthopaedic implant infections. *Adv. Drug Delivery Rev.* **2012**, *64*, 1165−1176.

(19) Lim, K.; Chua, R. R. Y.; Saravanan, R.; Basu, A.; Mishra, B.; Tambyah, P. A.; Ho, B.; Leong, S. S. J. Immobilization studies of an

DOI: 10.1021/acsomega.9b02614
ACS Omega 2019, 4, 18370−18380

engineered arginine−tryptophan-rich peptide on a silicone surface with antimicrobial and antibiofilm activity. *ACS Appl. Mater. Interfaces* **2013**, *5*, 6412−6422.
(20) Lee, M. H.; Brass, D. A.; Morris, R.; Composto, R. J.; Ducheyne, P. The effect of non-specific interactions on cellular adhesion using model surfaces. *Biomaterials* **2005**, *26*, 1721−1730.
(21) Crawford, G. A.; Chawla, N.; Das, K.; Bose, S.; Bandyopadhyay, A. Microstructure and deformation behavior of biocompatible TiO2 nanotubes on titanium substrate. *Acta Biomater.* **2007**, *3*, 359−367.
(22) Soumya, S.; Sreerekha, P. R.; Menon, D.; V. Nair, S.; Chennazhi, K. P. Generation of a biomimetic 3D microporous nanofibrous scaffold on titanium surfaces for better osteointegration of orthopedic implants. *J. Mater. Chem.* **2012**, *22*, 1904−1915.
(23) Lin, K.; Xia, L.; Gan, J.; Zhang, Z.; Chen, H.; Jiang, X.; Chang, J. Tailoring the Nanostructured Surfaces of Hydroxyapatite Bioceramics to Promote Protein Adsorption, Osteoblast Growth, and Osteogenic Differentiation. *ACS Appl. Mater. Interfaces* **2013**, *5*, 8008−8017.
(24) George, J.; Klika, A. K.; Higuera, C. A. Use of Chlorhexidine Preparations in Total Joint Arthroplasty. *J. Bone Joint Infect.* **2017**, *2*, 15−22.
(25) Weinstein, R. A.; Milstone, A. M.; Passaretti, C. L.; Perl, T. M. Chlorhexidine: Expanding the Armamentarium for Infection Control and Prevention. *Clin. Infect. Dis.* **2008**, *46*, 274−281.
(26) Barros, J.; Grenho, L.; Fernandes, M. H.; Manuel, C. M.; Melo, L. F.; Nunes, O. C.; Monteiro, F. J.; Ferraz, M. P. Anti-sessile bacterial and cytocompatibility properties of CHX-loaded nanohydroxyapatite. *Colloids Surf., B* **2015**, *130*, 305−314.
(27) Tallury, P.; Alimohammadi, N.; Kalachandra, S. Poly(ethylene-co-vinyl acetate) copolymer matrix for delivery of chlorhexidine and acyclovir drugs for use in the oral environment: Effect of drug combination, copolymer composition and coating on the drug release rate. *Dent. Mater.* **2007**, *23*, 404−409.
(28) Daud, N. M.; Masri, N. A.; Malek, N. A. N. N.; Abd Razak, S. I.; Saidin, S. Long-term antibacterial and stable chlorhexidine-polydopamine coating on stainless steel 316L. *Prog. Org. Coat.* **2018**, *122*, 147−153.
(29) Chen, K.; Caldwell, W. B.; Mirkin, C. A. Fullerene self-assembly onto $(MeO)_3Si(CH_2)_3NH_2$-modified oxide surfaces. *J. Am. Chem. Soc.* **1993**, *115*, 1193−1194.
(30) Chen, J. L.; Wang, J.; Qi, P. K.; Li, X.; Ma, B. L.; Chen, Z. Y.; Li, Q. L.; Zhao, Y. C.; Xiong, K. Q.; Maitz, M. F.; Huang, N. Biocompatibility studies of poly(ethylene glycol)-modified titanium for cardiovascular devices. *J. Bioact. Compat. Polym.* **2012**, *27*, 565−584.
(31) Chen, J. L.; Cao, J. J.; Wang, J.; Maitz, M. F.; Guo, L.; Zhao, Y. C.; Li, Q. L.; Xiong, K. Q.; Huang, N. Biofunctionalization of titanium with PEG and anti-CD34 for hemocompatibility and stimulated endothelialization. *J. Colloid Interface Sci.* **2012**, *368*, 636−647.
(32) Kozlovsky, A.; Artzi, Z.; Moses, O.; Kamin-Belsky, N.; Greenstein, R. B.-N. Interaction of Chlorhexidine With Smooth and Rough Types of Titanium Surfaces. *J. Periodontol.* **2006**, *77*, 1194−1200.
(33) Daud, N. M.; Bahri, I. F. S.; Malek, N. A. N. N.; Hermawan, H.; Saidin, S. Immobilization of antibacterial chlorhexidine on stainless steel using crosslinking polydopamine film: Towards infection resistant medical devices. *Colloids Surf., B* **2016**, *145*, 130−139.
(34) Rosenfeld, Y.; Lev, N.; Shai, Y. Effect of the Hydrophobicity to Net Positive Charge Ratio on Antibacterial and Anti-Endotoxin Activities of Structurally Similar Antimicrobial Peptides. *Biochemistry* **2010**, *49*, 853−861.
(35) Kim, T. S.; Park, S. H.; Park, D.; Lee, J. H.; Kang, S. Surface immobilization of chlorhexidine on a reverse osmosis membrane for in-situ biofouling control. *J. Membr. Sci.* **2019**, *576*, 17−25.
(36) Matinlinna, J. P.; Lassila, L. V. J.; Vallittu, P. K. The effect of five silane coupling agents on the bond strength of a luting cement to a silica-coated titanium. *Dent. Mater.* **2007**, *23*, 1173−1180.
(37) Sculean, A.; Gruber, R.; Bosshardt, D. D. Soft tissue wound healing around teeth and dental implants. *J. Clin. Periodontol.* **2014**, *41*, S6−S22.
(38) Wagner, V. E.; Koberstein, J. T.; Bryers, J. D. Protein and bacterial fouling characteristics of peptide and antibody decorated surfaces of PEG-poly(acrylic acid) co-polymers. *Biomaterials* **2004**, *25*, 2247−2263.
(39) Albers, C. E.; Hofstetter, W.; Siebenrock, K. A.; Landmann, R.; Klenke, F. M. In vitro cytotoxicity of silver nanoparticles on osteoblasts and osteoclasts at antibacterial concentrations. *Nanotoxicology* **2013**, *7*, 30−36.
(40) Saidin, S.; Chevallier, P.; Abdul Kadir, M. R.; Hermawan, H.; Mantovani, D. Polydopamine as an intermediate layer for silver and hydroxyapatite immobilisation on metallic biomaterials surface. *Mater. Sci. Eng., C* **2013**, *33*, 4715−4724.
(41) Gottenbos, B.; van der Mei, H. C.; Klatter, F.; Nieuwenhuis, P.; Busscher, H. J. In vitro and in vivo antimicrobial activity of covalently coupled quaternary ammonium silane coatings on silicone rubber. *Biomaterials* **2002**, *23*, 1417−1423.
(42) Li, X.; Gao, P.; Tan, J.; Xiong, K.; Maitz, M. F.; Pan, C.; Wu, H.; Chen, Y.; Yang, Z.; Huang, N. Assembly of Metal−Phenolic/Catecholamine Networks for Synergistically Anti-Inflammatory, Antimicrobial, and Anticoagulant Coatings. *ACS Appl. Mater. Interfaces* **2018**, *10*, 40844−40853.
(43) Chen, J.; Huang, N.; Li, Q.; Chu, C. H.; Li, J.; Maitz, M. F. The effect of electrostatic heparin/collagen layer-by-layer coating degradation on the biocompatibility. *Appl. Surf. Sci.* **2016**, *362*, 281−289.

DOI: 10.1021/acsomega.9b02614
ACS Omega 2019, 4, 18370−18380